Chapter 4

Influence of hexanol on the structure of CTAB-DNA and CTAB-SHN-DNA complexes

4.1 Introduction

This chapter deals with the structural transformations of CTAB-DNA complexes induced by the cosurfactant hexanol. Earlier work on lipid-DNA systems [1] has shown that hexanol can transform these complexes from a lamellar to a hexagonal structure, which has been attributed to the increased flexibility of the membranes in the presence of the cosurfactant. These experimental studies are described in section 4.2. The phase behaviour of a surfactant-water system is significantly altered by the addition of a cosurfactant and the phase diagram of the CTAB-hexanol-water system is also discussed in section 4.2. In section 4.3, we outline some theoretical calculations on the phase behaviour of lipid-DNA complexes as a function of the membrane flexibility, charge density and spontaneous curvature. In section 4.4, we present our results on CTAB-hexanol-DNA complexes. Novel structural transformations of these complexes are found driven by hexanol and DNA concentrations. We have also studied the influence of hexanol on the lamellar phase of CTAB-SHN-DNA complexes. Here again we find a transition from a lamellar to a hexagonal phase on increasing the hexanol concentration. These observations are dealt with in section 4.5. In section 4.6, we present some plausible explanations for the observed behaviour, based on the theories of phase behaviour of lipid-DNA complexes. Finally, section 4.7 deals with the conclusions

that may be drawn from the experiments discussed in this chapter.

4.2 Influence of a cosurfactant on the phase behaviour of surfactant-water systems

A cosurfactant is an amphiphile which does not form aggregates by itself in aqueous solutions. However when added to a surfactant solution, it modifies the properties of the surfactant aggregates such as their spontaneous curvature and flexibility. The effect of alcohols (ethanol to hexanol) on the micellar properties have been studied using conductivity, osmometry and light scattering techniques [2]. These studies indicate that long chain alcohols significantly affect the micellar properties. It is found that the addition of alcohols ranging from butanol to hexanol to a micellar solution results in a decrease of the critical micellar concentration (CMC) and of the molecular weight of the micelle, as well as an increase in the degree of ionization of the micelle. These are attributed to changes in surface charge density as well as in the dielectric constant near the head-group region.

The effect of long chain alcohols on surfactant systems has been studied in detail [3]. The morphology of the micelle is found to vary on adding hexanol and has been monitored through viscosity and light scattering measurements. Hexanol induces a sphere to rod transition of the micelles. This is a consequence of the decrease in spontaneous curvature of the headgroup-water interface in the presence of hexanol which leads to the elongation of micelles. These studies have also shown that the solution consists of long, flexible rod-like micelles that get entangled leading to a viscoelastic behaviour [4]. These are referred to as worm-like micelles in the literature.

The cetyltrimethylammonium bromide (CTAB)-water system exhibits an isotropic phase formed by spherical or rod-like micelles at low surfactant concentration (up to 25% by weight) [5]. On increasing the surfactant content, a hexagonal phase consisting of rod-like

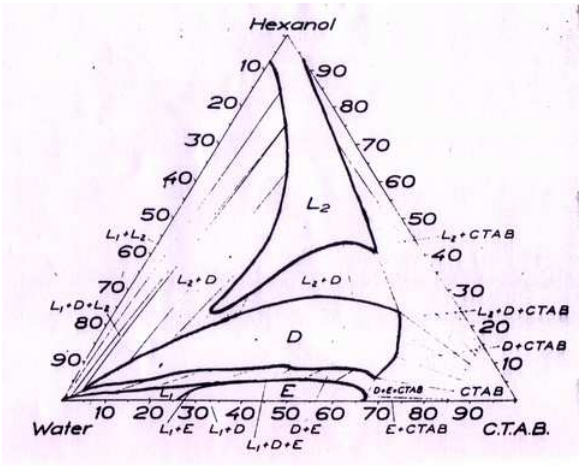

Figure 4.1: Phase diagram of CTAB-hexanol-water at 25^oC. L_1 - isotropic, aqueous solution ,L_2 - isotropic hexanol rich solution. D- lamellar phase, E- hexagonal phase [6].

micelles arranged on a 2D hexagonal lattice is obtained. The hexagonal phase persists over a large range of surfactant concentration. A lamellar phase finally appears at very high surfactant content (84-92% by weight). The addition of hexanol, however, alters the phase behaviour of CTAB-water system significantly.

The phase behaviour of CTAB-hexanol-water system (fig 4.1) has been probed in some detail using x-ray diffraction and polarizing microscopy [6]. An isotropic micellar solution is present at low surfactant and hexanol concentration (L_1). At higher surfactant concentrations (30- 70%) and low hexanol concentration (0 - 5%), a hexagonal phase (E) is observed. The incorporation of hexanol does not significantly alter the lattice parameter of the hexagonal phase, the diameter of the micellar cylinders and the thickness of the water layer up to 6% hexanol. At higher hexanol concentrations, a lamellar phase (D) is observed. The bilayer thickness is found to decrease from 3 nm to 2.5 nm on varying the ratio of hexanol to CTAB from 0.5 to 3.0. The lamellar phase exists up to 99% water dilution. This swelling behaviour is attributed to a steric repulsion arising from the thermal undulations of the bilayers, as discussed in chapter 2 [7]. The region L_2 observed at high hexanol concentrations, consists of a homogenous, isotropic phase rich in hexanol.

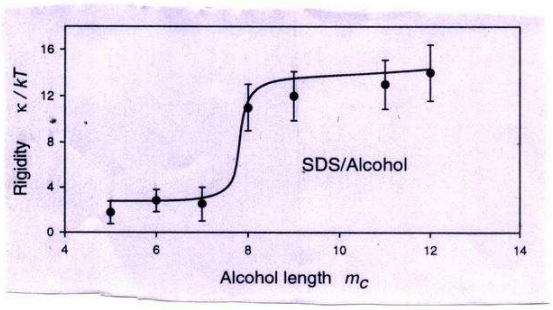

Figure 4.2: Bending rigidity of the bilayers in sodium dodecylsulphate-alcohol-water system as a function of alcohol chain length. Black circles are experimental data [8] and the solid line is calculated from theory [13].

The influence of alcohols on the bilayer bending rigidity (κ) has been studied using x-ray scattering techniques on sodium dodecylsulphate (SDS)-alcohol-water systems [8]. Due to the thermal undulations of the bilayers in the lamellar phase , the profile of the diffraction peak follows a power law behaviour given by

$I(0,q_z) \sim | q_z - q_m |^{-2+\eta_m}$

$I(q_\perp, 0, q_m) \sim (q_\perp)^{-4+2\eta_m}$

where $q_\perp$ and q_z are components of the wave vector **q** parallel and normal to the bilayers. $q_m = mq_o = 2\pi m/d$, m being an integer and d the lamellar periodicity.

η_m is the exponent which describes the algebraic decay of layer correlations and is given by $\eta_m = m^2 q_o^2 k_B T / 8\pi (BK)^{\frac{1}{2}}$, where B is the compressibility modulus and K the bending rigidity modulus of the lamellar phase. $K = \kappa / d$, where κ is the bending rigidity of a single bilayer. B can be estimated from osmotic pressure measurements on the lamellar phase. Thus from the power law exponent η_m, κ has been calculated [9]. The plot κ as a function of the alcohol chain length is given in fig 4.2. For short chain alcohols (up to heptanol) $\kappa \approx 3\ k_B T$, whereas for long chain alcohols (octanol to dodecanol) $\kappa \approx 13\ k_B T$.

Elasticity theory predicts that $\kappa \propto \delta^3$, where δ is the thickness of the membrane [10]. In some of the earlier microscopic theories of the bilayer bending rigidity [11, 12], the dramatic lowering of κ observed on addition of short hydrocarbon chains to a bilayer composed of

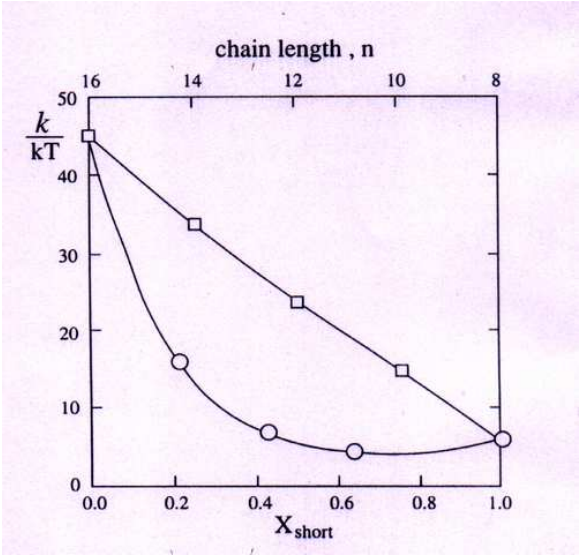

Figure 4.3: Bending elastic constants of a mixed bilayer consisting of long (C_{16}) and short (C_8) chains as a function of the short chain mole-fraction (circles, lower abcissa). Also shown (squares, upper abcissa) are the bending constants of a single component bilayer as a function of chain length. All data, for both the mixed and the pure bilayers are for chains packed with an average area per head-group of A = 31.6 Å^2. In these calculations the bending takes place at constant A [11].

long chains (fig 4.3) is qualitatively explained as follows: Closer to the hydrocarbon-water interface, the short and long chains have similar area per molecule. But beyond the region where the short chains terminate, the area per long chain increases and the bending in this region has negligible energy cost. Thus the short cosurfactant chains can be regarded as spacers between the long chains. Though these theories can explain the increase in κ with the chain length of the alcohol, they cannot account for the observed discontinuity in the bending rigidity with chain length. A more recent theory proposed by Foret and Wurger [13] is however able to quantitatively account for the measured rigidity as well as the discontinuous behaviour of bending modulus (fig 4.2).

4.3 Theoretical studies on the phase behaviour of cationic lipid-DNA complexes

The phase behaviour of solutions containing DNA, cationic and neutral lipids has been theoretically studied [14]. The different phases considered in this theory are intercalated lamellar structure of the lipid-DNA complex (L_α^C) consisting of DNA strands sandwiched between bilayers, the inverted hexagonal phase of the complex consisting of DNA covered by lipid monolayer (H_{II}^C), free bilayers in aqueous solution (L_α), uncomplexed, free DNA in solution (D) and inverted hexagonal phase (H_{II}). The free energies of the various phases have been calculated as a function of lipid composition and lipid/DNA ratio (ρ) .

The free energy per lipid molecule is of the form

$f_\alpha = f_\alpha^{es} + f_\alpha^{el} + f_\alpha^{mix}$ ($\alpha = L_\alpha^C, H_{II}^C, L_\alpha, H_{II}$)

The three terms represent contributions from electrostatic charging, elastic curvature, and 2D mixing entropy of the lipid layers respectively. The total free energy, which is a weighted sum involving the different phases, is then minimized with respect to the relevant thermodynamic variables to obtain the phase diagram.

The major contribution in the electrostatic free energy is the entropy gain from the release of counter ions originally bound to the polyion and the bilayers, into the solution on complex formation. This depends on the surface charge densities of the individual macroions, structure and composition of the condensed phases and salt concentration in solution. The electrostatic free energies of the various structures are calculated based on the nonlinear Poisson-Boltzmann (PB) equation.

If σ is the local surface charge density , Φ the corresponding electrostatic potential, V the volume of the electrolyte solution and n_0 the concentration of salt in the aqueous solution

and Ψ the reduced electrostatic potential given by $\Psi = e\Phi/k_BT$. The electrostatic free energy of a charged surface in solution is given by

$$F^{es} = \frac{1}{2}\int_S \sigma\Phi ds + k_BTn_0\int_v[\Psi sinh\Psi - 2cosh\Psi + 2]dv$$

where the first term involves contribution from all the charged surfaces S. Ψ is obtained by solving the Poisson-Boltzmann equation given by

$\nabla^2\Psi = \kappa'^2 sinh\Psi$

where the Debye screening length $\lambda_D = 1/\kappa'$.

The solution to the Poisson Boltzmann equation depends on the charged surface considered and boundary conditions specified for the system. In the L_α phase, the bilayer surfaces are treated as cationic, electrostatically decoupled surfaces for which $\Psi' = d\Psi/dz = 0$ at z $\rightarrow \infty$ and $\Psi' = -4\pi\phi_B l_B/a$ at the charged surface. l_B is the Bjerrum length and $\phi_B = N_B^+/N_B^0$, where N_B^+ and N_B^0 are the number of cationic and neutral lipids in the bilayer. If A is the cross-sectional area per lipid molecule, ϕ_B determines the surface charge density σ_B of the bilayer, given by σ_B = e ϕ_B/A.

In this model the ds DNA is treated as a cylindrical rod of uniform negative charge. Hence in the H_{II}^C, H_{II} and D phases, the charged surfaces are cylindrically symmetric.If b is the separation between the charges on the DNA, then the uniform surface charge density of DNA, σ_D, may be given in terms of the radius of DNA R_D as σ_D = - e / 2 π R_D b. Thus for phase D, the boundary condition is given by $\Psi' = 0$ at r = ∞, and $\Psi'(R_D) = 2l_B/(R_D)b$ at the surface of the rod. For the H_{II} phase, the boundary conditions are $\Psi'(0) = 0$ and $\Psi'(R_I) = 4\pi\phi_I l_B/A_{hg}$, where R_I is the radius of curvature of the lipid head group water interface in the H_{II} phase and A_{hg} is the head group area of the lipid molecule in the inverted phase, and $\phi_I = N_I^+/N_I^0$ where N_I^+ and N_I^0 are the number of cationic and neutral lipids in the inverted hexagonal phase. For the H_{II}^C phase, the PB equation is solved for the aqueous region between two concentric, oppositely charged surfaces with $R_D \leq r \leq R_H$. R_H is the radius of curvature of the strongly curved lipid head group surface in the H_{II}^C phase.

$R_H = R_D + \delta_w$, where δ_w is the thickness of the water layer between the DNA and the lipid molecules. The boundary conditions are $\Psi'(R_D) = 2l_B/R_D b$ at the DNA surface and $\Psi'(R_H) = 4\pi\phi_H l_B/A_{hg}$ at the lipid surface, where A_{hg} is the head group area of the lipid molecule in the inverted phase and $\phi_H = N_H^+/N_H^0$, where N_H^+ and N_H^0 are the number of cationic and neutral lipids in the inverted hexagonal lipid -DNA complex.

The PB equation for the unit cell of the L_α^C phase is two dimensional and the boundary conditions here are more complex [15].

The elastic energy density of the lipid monolayers constituting the different lipid containing phases is given by

$f^{el}(c,\phi) = \mathrm{A}(\kappa/2)(c - c_o(\phi))^2 + f_v.$

The first term represents the elastic deformation energy per molecule in a cylindrically bent lipid monolayer. Here, κ is the bending modulus, c_o the spontaneous curvature of the monolayer, c the actual curvature and A the area per molecule. ϕ denotes the lipid composition. In the inverted phase, some of the hydrophobic tails are more stretched in order to fill the interstitial regions between the cylinders. Since these molecules experience a different geometry from the rest, they are frustrated and experience average stretching cost per molecule given by f_v. For the phases L_α and L_α^C, f_v is zero.

The monolayers in the different phases are assumed to be ideal 2D mixtures. Hence their mixing free energy is given by

$f^{mix}/k_BT = \phi ln\phi + (1-\phi)ln(1-\phi)$

Adding the electrostatic, elastic, and mixing contributions, the total free energy of the mixture is minimized with respect to the relevant variables. It involves eleven concentration variables, of which three are eliminated due to the conservation condition that the total number of cationic lipid, neutral lipid and DNA molecules are fixed. Also since R_H and R_I are fixed in the inverted phases, it imposes a structural constraint that fixes the number of molecules that can be incorporated into the inverted phase. Thus f is a function of seven

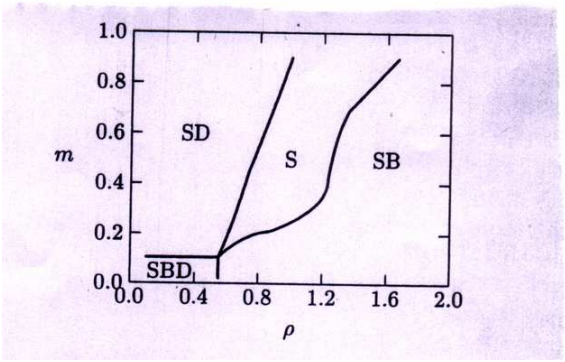

Figure 4.4: The phase diagram of a lipid-DNA mixture, for lipids that self-assemble into rigid planar membranes. The phase diagram was calculated for a membrane characterized by $\kappa = 10k_B$T and $c_o = 0$. The symbols S,B, and D denote, respectively, the L_α^C, L_α and uncomplexed DNA phases [14].

independent variables. For every ρ, which is the ratio between the total number of cationic and DNA charges in the system, and m, the mole fraction of the cationic lipid in the original lipid mixture, the minimization of free energy with respect to these variables gives the number and identity of the coexisting phases and their composition.

For rigid planar membranes, no hexagonal phases appear in the calculated phase diagram (fig 4.4). At low values of ρ, lamellar complexes coexist with uncomplexed DNA. Here the DNA-DNA separation remains constant. Further increase of ρ leads to a one-phase region of lamellar complex alone where the DNA-DNA separation increases linearly with ρ, near the isoelectric point. At high values of ρ the complex coexists with excess bilayers.

For soft planar membranes, a more complex phase behaviour is obtained (fig 4.5). At small values of ρ, D coexists with either L_α^C or H_{II}^C depending on the value of m. At high ρ, all the DNA is complexed and coexists with excess bilayers. The lamellar phase of the complex, persists over a large range of ρ at high m, since the structure can tolerate changes in lipid composition by adjusting d_{DNA}. Due to the structural constraint imposed in the H_{II}^C phase, it exists only along a straight line in the phase diagram. At fixed ρ, the complex can undergo a transition from a lamellar to a hexagonal complex on decreasing the charge density which

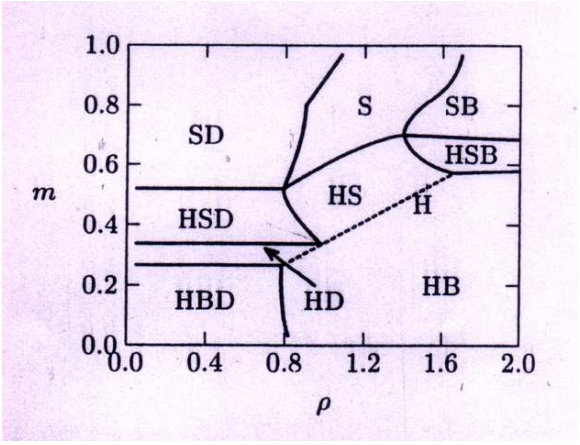

Figure 4.5: The Phase diagram of a lipid-DNA mixture, for lipids that self-assemble into very soft planar membranes. The phase diagram was calculated for membranes characterized by κ=0 and $f_v \equiv 0$. The symbols S,B,H and D denote respectively, the L_α^C,L_α,H_{II}^C and uncomplexed DNA phases. The straight dashed line marks the single H_{II}^C phase region [14].

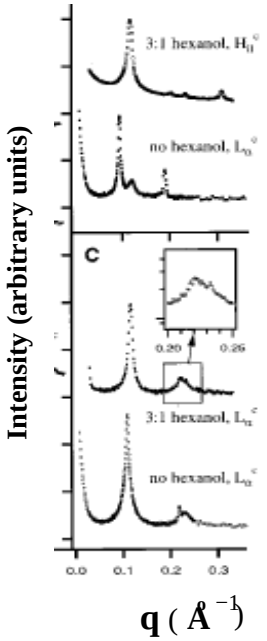

Figure 4.6: A series of SAXS scans of DOTAP-DOPC-hexanol-DNA complexes in excess water at different [hexanol]/[lipid] ratio [1].

has been observed experimentally [1]. A hexagonal to lamellar transition of the complex is also predicted for intermediate charge densities on decreasing ρ. Such transitions have not been reported in any of the earlier studies on lipid/surfactant-DNA complexes.

In the absence of DOPC, DNA-DOTAP-hexanol complexes exhibit a lamellar phase [1].

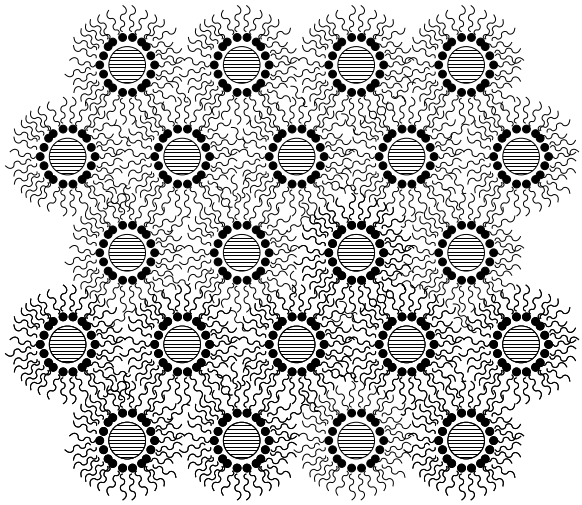

Figure 4.7: Schematic diagram of the inverted hexagonal phase (H_{II}^C) where the DNA are confined to the aqueous cores of the micelles.

The DNA-DNA separation was found to increase with hexanol concentration. Further, when [DOPC]/[DOTAP] ~ 1, the diffraction pattern indicates a 2D hexagonal lattice (fig 4.6) with the addition of hexanol. The lattice parameter of the hexagonal phase was found to be 6.25 nm. An inverted hexagonal structure consisting of DNA covered by a lipid monolayer, arranged on a 2D hexagonal lattice has been proposed in these systems (fig 4.7). As discussed above the addition of hexanol increases the flexibility of the bilayers. In addition, they also reduce the charge density. Therefore, these experimental observations are consistent with the $L_\alpha^C \rightarrow H_{II}^C$ transitions predicted for highly flexible bilayers with low charge density.

4.4 CTAB-DNA-hexanol Complexes

We have studied the influence of hexanol on the structure of CTAB-DNA complexes using small angle x-ray diffraction. The hexanol concentration β (=[hexanol]/[CTAB]) was varied from 1 to 10, keeping the concentration of CTAB fixed at 10 mM. All the complexes were found to be birefringent under a polarizing microscope, irrespective of the hexanol and DNA concentrations. The experimental results on CTAB-DNA-hexanol complexes may be summarized in the phase diagram (fig 4.8). This gives the structure of the complexes at

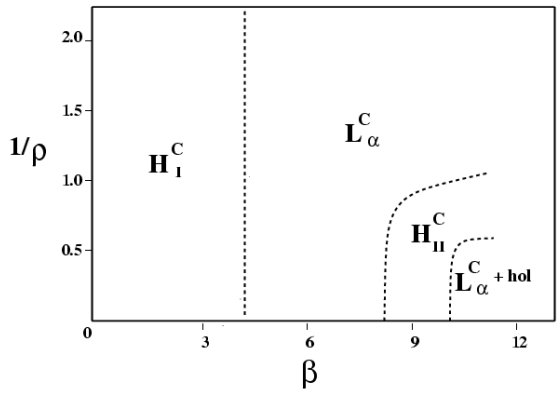

Figure 4.8: Partial phase diagram of the system showing the different structures obtained as a function of hexanol and DNA concentrations. β = [hexanol]/[CTAB], ρ = (wt. of CTAB)/(wt. of DNA). hol denotes the hexanol rich phase coexisting with the complex. The locations of the different phase boundaries have not been precisely determined.

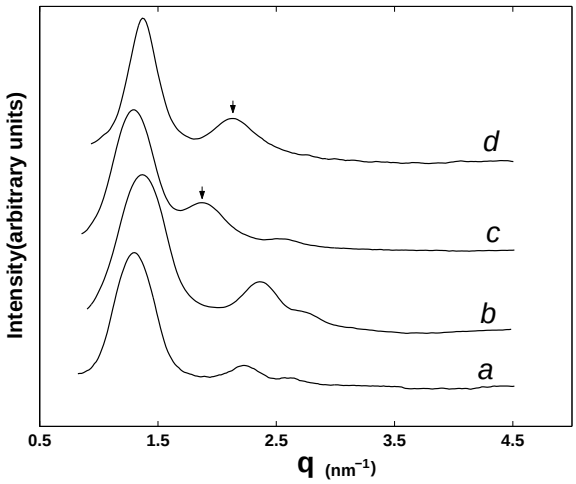

Figure 4.9: Diffraction patterns of the CTAB-hexanol-DNA complexes. β and ρ for the different curves are: 3.5, 36 (a) 3.5, 1 (b); 5, 36 (c); 5 ,1 (d); ρ_{iso}=1.12. CTAB concentration in the aqueous solution was 10 mM. The arrows on curves (c) and (d) indicate in-plane DNA-DNA correlation peak.

different hexanol and DNA concentrations. Note that β and ρ correspond to the total concentrations of hexanol and DNA in the solution and not in the complex alone. The boundaries between the different structures have not been determined very accurately.

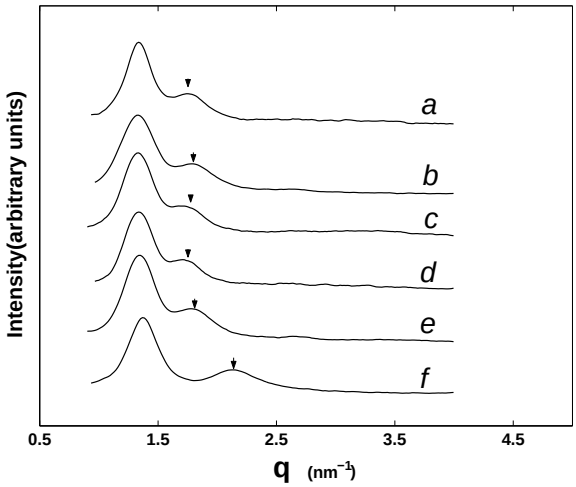

Figure 4.10: Diffraction patterns of the CTAB-hexanol-DNA complexes. β=8 and ρ for the different curves are: 36 (a); 7.2 (b); 1.8 (c); 1.2 (d); 1.01 (e); 0.9 (f); ρ_{iso}=1.12.

The x-ray diffraction data at low hexanol concentration (fig 4.9a,b) reveal three peaks in the small angle region, whose q values are in the ratio 1:$\sqrt{3}$:2. Hence they could be indexed as the (1,0),(1,1) and (2,0) reflections of a 2-D hexagonal lattice. This phase was observed up to β=3.5. The lattice parameter of the hexagonal phase decreases from 5.64 nm at β = 0 to 5.50 nm at β = 3.5 for ρ = 36. At a higher DNA concentration, (ρ= 1), the lattice parameter decreases to 5.23 nm from 5.5 nm at β =3.5 .

At $\beta \sim 5$, diffraction pattern consists of two peaks in the small angle region corresponding to a lamellar structure (fig 4.9c,d). A diffuse peak whose position depends significantly on the DNA concentration near the isoelectric point is also observed indicated by an arrow in the diffraction patterns. Similar observations have been made in CTAB-SHN-DNA complexes (chapter 3) and cationic lipid-DNA complexes [16] where an intercalated lamellar structure has been proposed consisting of DNA strands sandwiched between the bilayers. The peak whose position depends on DNA concentration arises due to the correlation between the DNA strands in the plane of the bilayers and gives the average distance d_{DNA} between adjacent DNA strands. At $\rho > \rho_{iso}$, d_{DNA} increases from 3.32 nm at β = 5 to 3.65 nm at β =8 (fig 4.10). The structure of the complex remains lamellar up to $\beta \sim 8.5$ (table 4.1).

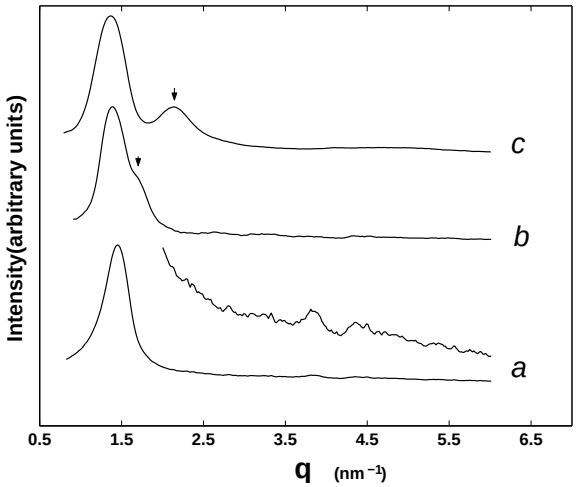

Figure 4.11: Diffraction patterns of the CTAB-hexanol-DNA complexes. β = 9 and ρ for the different curves are: 36 (a); 1 (b) 0.9 (c); ρ_{iso}=1.12. The peaks at q=3.85 and 4.4 nm^{-1} correspond to the (2,1) and (3,0) reflections from the 2-D hexagonal lattice.

At β = 8.5, another phase is observed at ρ = 36. The morphology of the complex changes at this hexanol concentration and it precipitates out of the aqueous solution. One strong peak and two weak reflections are observed in the diffraction pattern at $\beta \sim 9$ (fig 4.11a). The scattering vectors, q are in the ratio 1:$\sqrt{7}$:3. These reflections can be indexed as the (1,0), (2,1) and (3,0) reflections from a 2D hexagonal lattice. On decreasing ρ, a transition to a lamellar phase is observed close to ρ_{iso} and the peak positions indicated by an arrow (fig 4.11b,c) shift from 3.6 nm to $\sim$ 2.7 nm.

At β = 10, the surfactant solution phase separates to form surfactant rich and hexanol rich phases. On adding DNA to the CTAB-hexanol solution at β = 10, the complex obtained coexists with a hexanol rich phase. X-ray diffraction indicates a lamellar structure for the complex at ρ = 36 (fig 4.12a). A DNA-DNA peak is observed at 3.7 nm which is similar to that observed at lower values of β. However, further decrease in ρ leads to the gradual disappearance of the hexanol rich phase (hol) and at ρ = 1, a hexagonal phase is observed (fig 4.12b). On increasing DNA concentration much beyond the isoelectric point a lamellar structure reappears (fig 4.12c) with a d_{DNA} of 2.96 nm. This transition occurs in a narrow range of $1 > \rho > 0.5$. Such transformations of the structure, driven by DNA concentration

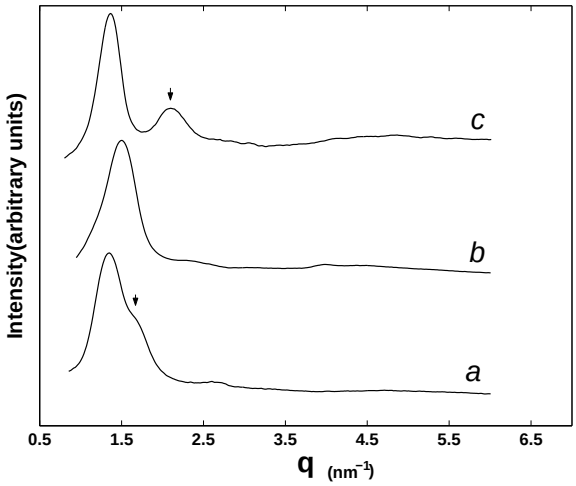

Figure 4.12: Diffraction patterns of the CTAB-hexanol-DNA complexes. β and ρ for the different curves are: 10, 36 (a); 10, 1 (b); 10, 0.5 (c); ρ_{iso}=1.12.

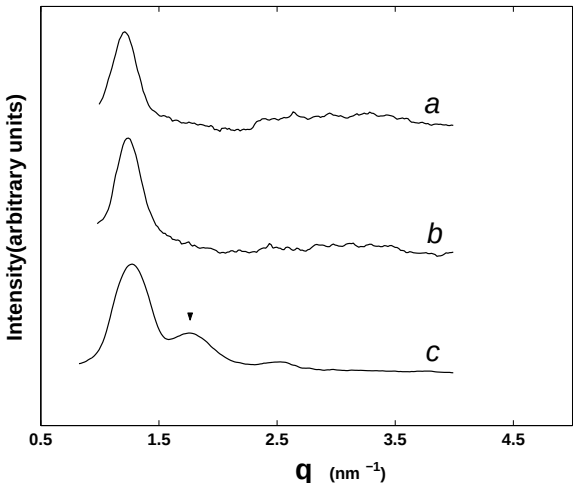

Figure 4.13: Diffraction patterns of the CTAB-SHN-hexanol-DNA complexes. α = 0.7; β and ρ for the different curves are: 3, 36 (a); 4, 36 (b) 5, 36 (c); ρ_{iso}=3.74.

have not been reported in the literature.

4.5 CTAB-SHN-hexanol-DNA Complexes

As discussed in chapter 3, CTAB-SHN-DNA complexes have a lamellar phase at [SHN]/[CTAB] ~ 0.6 . We have studied the influence of hexanol on these complexes. The diffraction pattern of CTAB-SHN-hexanol-DNA complexes reveal three peaks in the small angle region with the scattering vectors in the ratio, 1:2:3 (fig 4.13). Hence up to $\beta \sim 5$,

Table 4.1: The d-spacings, structure and lattice parameters of CTAB-hexanol-DNA complexes at different values of α and ρ. a and d denote the lattice parameters of the hexagonal and lamellar phases respectively. ρ_{iso} = 1.12.

β	ρ	$d_1(nm)$	$d_2(nm)$	$d_3(nm)$	$d_{DNA}(nm)$	phase	a, d(nm)
0	36	4.88	2.82	2.44	-	H_I^C	5.64
0	1	4.88	2.82	2.44	-	H_I^C	5.64
3.5	36	4.76	2.79	2.38	-	H_I^C	5.50
3.5	1	4.53	2.64	2.27	-	H_I^C	5.23
5	36	4.87	2.43	-	3.32	L_α^C	4.87
5	1	4.65	-	-	3.23	L_α^C	4.65
6	36	4.76	-	-	-	L_α^C	4.76
8	36	4.7	-	-	3.65	L_α^C	4.70
8	7.2	4.70	-	-	3.52	L_α^C	4.70
8	3.6	4.76	-	-	3.61	L_α^C	4.76
8	1.8	4.70	-	-	3.61	L_α^C	4.70
8	1.2	4.7	-	-	3.61	L_α^C	4.70
8	1.03	4.7	-	-	3.52	L_α^C	4.70
8	0.9	4.59	-	-	2.93	L_α^C	4.59
8.5	36	4.35	1.64			H_{Ii}^C	5.01
8.5	0.85	4.61			3.01	L_α^C	4.61
9	36	4.34	1.62	-	-	H_{Ii}^C	5.01
9	7.2	4.36	1.64	-	-	H_{Ii}^C	5.03
9	1	4.49	-	-	-		
9	0.9	4.59	-	-	2.96	L_α^C	4.59
10	36	4.60	2.30	-	3.7	L_α^C	4.60
10	1	4.17	1.58	-	-	H_{Ii}^C	4.82
10	0.47	4.5			2.97	L_α^C	4.5

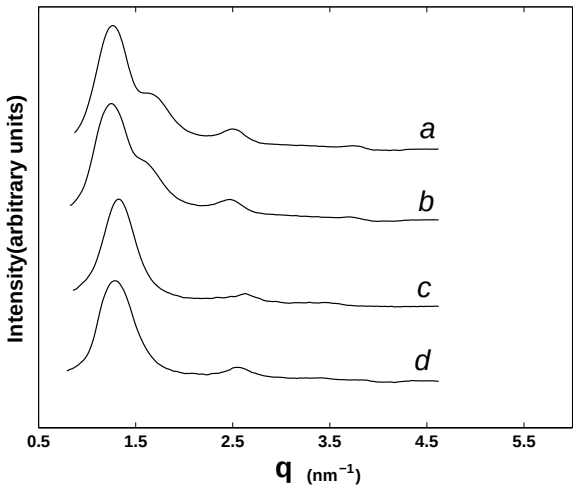

Figure 4.14: Diffraction patterns of the CTAB-SHN-hexanol-DNA complexes. α = 0.7; β and ρ for the different curves are: 6, 36 (a); 7, 36 (b); 8, 36 (c); 9, 36 (d); ρ_{iso} = 3.74.

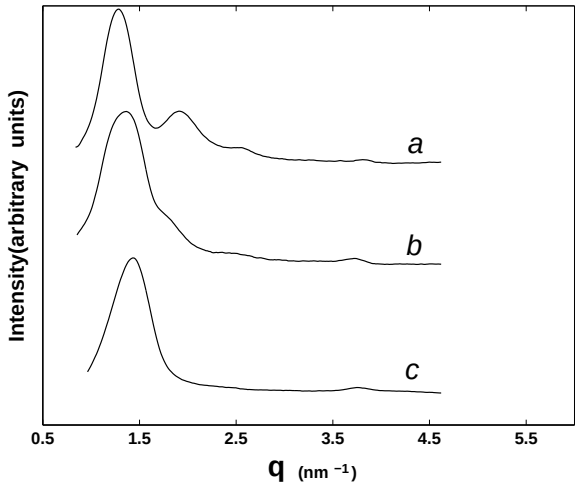

Figure 4.15: Diffraction patterns of the CTAB-SHN-hexanol-DNA complexes.α = 0.7; β and ρ for the different curves are: 10, 36 (a); 10, 1 (b) 12, 0.5 (c); ρ_{iso}=3.74.

the structure of the complex remains lamellar. Also, the lattice parameter decreases with increase in hexanol concentration (table 4.2). Phase separation occurs in the CTAB-SHN-hexanol solution at $\beta \sim 6$ with the appearance of a hexanol rich phase. At $\beta = 6$, the complex coexists with a hexanol-rich phase. However the complex remains lamellar up to $\beta = 9$ (fig 4.14). At $\beta = 10$, the complex shows a lamellar phase at low DNA concentrations (fig 4.15 a, b).

At $\beta \sim 10$, the morphology of the complex changes at high DNA concentration. It no longer remains dispersed in the aqueous solution but precipitates out of it. Further the hexanol rich phase disappears. Similar behaviour was also observed at $\beta \sim 12$. One strong reflection and a weak reflection were observed in the diffraction pattern of this complex (fig 4.15c), with the scattering vectors in the ratio, 1:$\sqrt{7}$. These could be indexed as the (1,0) and (2,1) peaks of a 2D hexagonal lattice. The d-spacings, lattice parameters and structures of the complexes at various SHN, hexanol and DNA concentrations are given below (table 4.2).

Table 4.2: The d-spacings,structure and lattice parameters of CTAB-SHN-Hexanol-DNA complexes at different values of β and ρ.

β	ρ	$d_1(nm)$	$d_2(nm)$	$d_3(nm)$	$d_{DNA}(nm)$	phase	a, d(nm)
0	14.4	5.54	2.77	1.85	-	L_α^C	5.54
0	3	5.54	2.77	1.85	-	L_α^C	5.54
1	36	5.32	-	-	-	L_α^C	5.23
3	36	5.19	-	-	-	L_α^C	5.19
4	36	5.06	-	-	-	L_α^C	5.06
5	36	4.93	2.47	-	3.55	L_α^C	4.93
6	36	4.99	2.50	1.66	3.71	L_α^C	4.99
7	36	5.06	2.53	1.69	3.93	L_α^C	5.06
8	36	4.70	2.35	-	-	L_α^C	4.70
9	36	4.87	2.43	-	-	L_α^C	4.87
10	36	4.93	2.47	1.64	3.32	L_α^C	4.93
10	1	4.6		-	-		
12	0.5	4.50	1.68	-	-	H_{II}^C	5.20

4.6 Discussion

In the absence of hexanol, CTAB-DNA complexes form an intercalated hexagonal phase (fig 4.16) as discussed in chapter 3. Hence the hexagonal structure at low hexanol concentrations can be expected to be the same. The decrease in the lattice parameters of the hexagonal phase on increasing β is a consequence of the thinning of micellar cylinders in the presence of hexanol. One can estimate the DNA/surfactant ratio in the H_I^C phase from the geometry. Each unit cell of the 2D hexagonal lattice, contains one micellar cylinder and two DNA strands. The ratio of weight of CTAB to the weight of DNA ρ_c, is given by

$\rho_c = A_m \rho_s f/(2\rho_D A_D)$

where A_m is the area of the micellar cylinder, ρ_s the density of the surfactant, f the weight fraction of CTAB in the micelle, A_D the average area occupied by the DNA and ρ_D the density of DNA.

From the lattice parameter a of the hexagonal phase and the radius of the hydrated DNA strand $R_D \sim 1.25$ nm, we can estimate the area of the micellar cylinder given by

$A_m = \pi(a - \sqrt{3}R_D)^2/3$

If ϕ_1 and ϕ_2 are the volume fractions of CTAB and hexanol molecules respectively in the

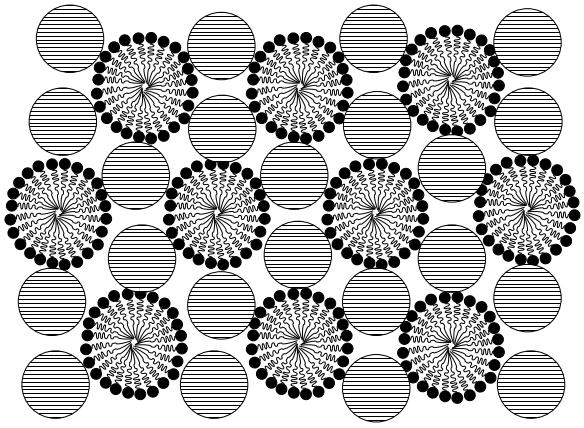

Figure 4.16: The intercalated hexagonal phase (H_I^C), where each DNA strand is surrounded by three cylindrical micelles.

surfactant solution, ρ_1 and ρ_2 the density of CTAB and hexanol, then $\rho_s = \phi_1\rho_1 + \phi_2\rho_2$ The average area of DNA, A_D [= molar volume/(N_A. contour length)] ~ 1.86 nm^2 . The density of DNA ρ_D is 1.7 g/cc and the weight fraction of CTAB in the micelle f is 0.51 at β = 3.5 . This gives ρ_s = 0.9 .

In the absence of hexanol ρ_c = 3.98. Since ρ_{iso}=1.1, this implies that these complexes are overcharged with excess CTAB. This is a consequence of the much smaller area of the CTAB head group compared to the effective area per charge of the DNA. The system would, therefore, tend to incorporate more DNA in the complex in order to achieve better neutralization. However, this can only be done by making the CTAB micelles thinner. The observation that the lattice parameter of these complexes do not change with DNA concentration indicates that such deformations are prevented by the rigidity of these micelles.

ρ_c = 1.67 at β = 3.5, which is still larger than ρ_{iso}. Interestingly, in this case the lattice parameter is found to decrease with DNA concentration for ρ < 1.67, indicating uptake of more DNA by thinning the cylindrical micelles. The incorporation of hexanol in the micelles seems to make them more flexible and susceptible to such deformations.

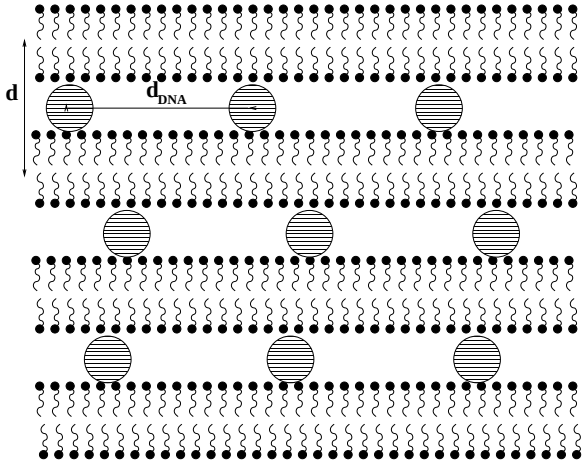

Figure 4.17: Schematic diagram of lamellar phase (L_α^C) of DNA-surfactant complexes,where the DNA strands (denoted by shaded circles) are sandwiched between surfactant bilayers.

The diffraction pattern of the lamellar phase observed at $\beta = 5$, indicates that the structure is similar to the intercalated lamellar phase (L_α^C), discussed in chapter 3 (fig 4.17) [16]. The lattice parameter of 4.9 nm observed at $\rho = 36$, is consistent with a CTAB-hexanol bilayer of thickness 2.4 nm and a hydrated DNA of diameter 2.5 nm. The decrease in the lamellar periodicity to $\sim$ 4.7 nm, at $\beta = 8$, indicates that the addition of hexanol leads to the thinning of bilayers. The increase in DNA-DNA separation by nearly 3 nm on varying β from 5 to 8 at low DNA concentrations ($\rho = 36$), is probably a consequence of a decrease in the charge density of the bilayers when it incorporates more hexanol. As discussed in section 3.2, addition of hexanol to CTAB-water system leads to a transition from a hexagonal to a lamellar phase. The transition from H_I^C to L_α^C on increasing the hexanol concentration is thus consistent with the phase behaviour of the surfactant-water system. The sharp decrease in d_{DNA}, near ρ_{iso} observed at $\beta \sim 8$ is similar to the behaviour observed in lipid-DNA complexes. Here below ρ_{iso}, the complex get overcharged with excess DNA due to the higher free energy of the uncomplexed DNA in solution [17].

The diffraction pattern (fig 4.11a) and the morphology of the complex indicates that the

hexagonal phase observed at $\beta = 8.5$, is different from that observed at lower values of β. An inverted hexagonal phase can be proposed for the complex. The lattice parameter of 5.05 nm is consistent with a CTAB-hexanol bilayer of thickness ~ 2.5 nm and the diameter of a hydrated DNA ~ 2.5 nm. A similar structure has been observed in lipid-DNA complexes in the presence of hexanol [1], where DNA strands are confined to the aqueous cores of inverted cylindrical micelles (fig 4.7). This (H_{II}^C) structure is consistent with the hydrophobic nature of the complex and is further supported by a simple analysis of the diffraction data. The absence of the (1 1) and (2 0) reflections in the diffraction patterns of the complex indicates that the form factor of the electron rich cylindrical core has a zero in between the corresponding values of q. Taking the electron density of the core to be uniform, this condition gives the radius of the core to be about 1.3 nm, which is very close to that of a hydrated DNA (~ 1.25 nm).

The occurrance of the $L_\alpha^C \rightarrow H_{II}^C$ transition on increasing the hexanol concentration may be qualitatively understood as follows. In the inverted phase, the neutralization of the base pairs by the surfactant counter ions is more efficient due to their enhanced proximity in this geometry. Hence formation of an inverted phase results in a gain in the electrostatic contribution to the free energy. However the accompanying energy cost for bending the bilayer around the DNA is given by $\frac{1}{2}\kappa\,(C - C_o)^2$. C is the curvature of the DNA cylinder and C_o the spontaneous curvature of the surfactant-water interface. The presence of hexanol is known to lower κ and hence decreases the energy cost for bending the bilayers [8]. It has been shown from theoretical computations that H_{II}^C phase is preferred over the L_α^C phase in lipids with very flexible bilayers at low charge density [14]. The presence of hexanol decreases the charge density of the bilayers as well as increases their flexibility and hence satisfies both these conditions. Further, as hexanol is not confined to the lipid-water interface, it can occupy the interstitial regions in the H_{II}^C structure where the three inverted cylindrical micelles meet. This reduces the frustration of the chains of the amphiphile that would have had to stretch in order to occupy these regions. Thus the presence of hexanol further stabilizes the

H_{II}^C phase.

The diffraction pattern as well as the morphology of the complexes obtained at higher DNA concentration when $\beta = 9$ indicates that they form an intercalated lamellar structure. The reason for the transition from H_{II}^C to L_α^C structure on increasing DNA concentration observed here, is most likely the denser packing of DNA in the lamellar phase. The distance between two adjacent DNA is fixed at the lattice parameter *a*, in the inverted phase. On the other hand, no such restriction exists in the L_α^C structure, and d_{DNA} can change significantly across the isoelectric point. The amount of DNA which can be incorporated into lamellar phase as compared to the inverted hexagonal phase, can be estimated from the geometry of the two structures. For the inverted hexagonal phase, it is given by

$\rho_c^H = \rho_s^1 \, A_s^1 \, f^1 / \rho_D \, A_D.$

where the superscript 1 denotes the H_{II}^C structure.

Similarly for the lamellar complex it is given by

$\rho_c^L = \rho_s^2 \, A_s^2 \, f^2 / \rho_D \, A_D.$

where the superscript 2 denotes the L_α^C structure.

If we consider the two structures at similar surfactant composition,

$\rho_s^1 \, f^1 = \rho_s^2 \, f^2,$

$\rho_c^H / \rho_c^L = A_s^1 / A_s^2$

Since $A_s^1 = (\sqrt{3}a^2 - 2\pi R_D^2)/2$ and A_s^2, estimated from the bilayer thickness δ and the separation between the DNA strands d_{DNA}, is given by $A_s^2 = d_{DNA} \, \delta$.

The ratio, $\rho_c^H / \rho_c^L = (\sqrt{3}a^2 - 2\pi R_D^2)/(2\delta d_{DNA})$. Putting a= 5.0 nm, R_D = 1.25 nm, and δ= 2.2 nm, this ratio turns out to be $7.5/d_{DNA}$. Hence the lamellar complex can accommodate more DNA than the H_{II}^C structure as long as $d_{DNA} < 7.5$ nm. In the lamellar complexes obtained for low hexanol concentrations, d_{DNA} is 3.5 nm even at low hexanol concentrations.

Thus it is clear that more DNA can be accommodated in the L_α^C phase as compared to H_{II}^C.

Though at low DNA concentrations, the H_{II}^C phase is stabilized by the efficient neutralization of DNA, it becomes unstable in the presence of excess uncomplexed DNA and transforms to L_α^C. The fact that the $H_{II}^C \rightarrow L_\alpha^C$ transition is observed at a value of ρ slightly greater than ρ_{iso} supports the proposed mechanism. Such transformations of the structure of the complexes, driven by DNA concentrations have not been reported in the literature.

The DNA concentration at the H_{II}^C to L_α^C transition should correspond to the maximum amount of DNA that can be incorporated in the former structure. As discussed earlier, it can be estimated from the geometry of the system and is given by $\rho_c = (\sqrt{3}a^2 - 2\pi R^2)\rho_s f/(2A_D\rho_D)$. At $\beta = 9$, ρ_c is found to be 1.3. This is close to the experimental value of ~ 1.0, thus once again confirming the above mechanism.

The formation of a lamellar complex at $\beta = 10$ for high ρ with d_{DNA} comparable to the values at lower β and high ρ, indicates that the hexanol concentration in the surfactant-rich phase is less than that in the solution just before phase separation. The gradual disappearance of the hexanol rich phase on increasing the DNA concentration indicates that hexanol content in the complex increases. This leads to an increase in the flexibility and a decrease in charge density of the bilayer and the structure transforms to H_{II}^C. The $H_{II}^C \rightarrow L_\alpha^C$ transition at higher DNA concentration as before is driven by the denser packing of DNA in the latter phase. The observed d_{DNA} of 2.9 nm is consistent with this. The narrow range of $0.5 < \rho < 1$ over which the transition occurs agrees with the estimated $\rho_c \sim 1.0$.

Similar phase transitions have been theoretically predicted for soft bilayers ($\kappa = 0$) at intermediate charge densities [14]. Here the charge density of the bilayers are varied using a mixture of the cationic and neutral lipids. Since both the lipids remain near the lipid-water interface, from the lipid composition and the head group area of the lipids, the charge density

of the bilayers at each composition can be estimated. Such an estimation cannot be made in our system since the hexanol does not remain confined at the surfactant-water interface. Hence the phase diagram obtained for the CTAB-hexanol-DNA complexes cannot be quantitatively compared with the calculated phase diagrams of lipid-DNA complexes. However our experimental observations qualitatively agree with the theoretical prediction of $H_{II}^C \rightarrow L_\alpha^C$ transition in flexible bilayers at low charge densities on increasing the DNA concentration.

In the CTAB-SHN-hexanol-DNA complexes, the structure remains lamellar for all hexanol concentrations, at high values of ρ. The decrease in the lattice parameters on increasing β, observed before the phase separation occurs in the surfactant solution, is consistent with the thinning of bilayers in the presence of hexanol. Similar to the lipid-DNA complexes, a transition from $L_\alpha^C \rightarrow H_{II}^C$ is also observed in these complexes at high ρ. The absence of (1,1) and (2,0) reflections and the presence of a weak (2,1) reflection confirms the inverted phase. Though a detailed study of the system has not been carried out, the phase behaviour of this system can be expected to be similar to that of CTAB-hexanol-DNA complexes, except for the occurrance of the intercalated hexagonal structure at low hexanol concentrations in the latter system.

4.7 Conclusion

We have studied the influence of hexanol on the structure of complexes of CTAB formed with ds DNA. At low DNA concentrations, the complexes exhibit a $H_I^C \rightarrow L_\alpha^C \rightarrow H_{II}^C$ transition on varying the hexanol concentration. These transitions are in accordance with the known influence of hexanol on the structure and properties of CTAB aggregates. A novel $H_{II}^C \rightarrow L_\alpha^C$ transformation is observed as a function of DNA concentration at high hexanol content, which may be understood in terms of the more efficient packing of DNA in the L_α^C

structure. A partial phase diagram of this system has been constructed, which shows the different structures exhibited by these complexes. We have also studied the influence of hexanol on the structure of CTAB-SHN-DNA complexes. The phase behaviour of the system is found to be similar to the CTAB-DNA complexes, but for the occurrance of the intercalated hexagonal phase at low hexanol concentration in the former system.

Bibliography

[1] I. Koltover, T. Salditt, J. O. Raedler, and C. R. Safinya, Science, **281**, 78 (1998).

[2] R. Zana, S. Yiv, C. Strazielle, and P. Lianos, J. Colloid Interface Sci **80**, 208 (1981).

[3] R. Gomati, J. Appell, P. Bassereau, J. Marignan,and G. Porte,J. Phys. Chem., **91**, 6203 (1987).

[4] J. Appell, G. Porte, and Y. Poggi, J. Colloid Interface Sci **87**, 492 (1982).

[5] F. Husson, H. Mustachchi, and V. Luzzati, Acta Cryst. **13**, 668 (1960).

[6] P. Ekwall, L. Mandell, and K. Fontell, J. Colloid Interface Sci **29**, 639 (1969).

[7] W. Helfrich, Z. Naturforsch, **33a**, 305 (1978).

[8] C. R. Safinya, E. B. Sirota, D. Roux, and G. S. Smith, Phys. Rev. Lett., **62**, 1134 (1989).

[9] D. Roux and C. R. Safinya, J. Phys. France **49**, 307 (1998)

[10] L. D.Landau and E.M.Lifschitz, *Theory of Elasticity* (Pergamon, New York, 1970).

[11] I. Szleifer, D. Kramer, A. Ben-Shaul, D. Roux, and W. M. Gelbart, Phys. Rev. Lett., **60**, 1966 (1988).

[12] I. Szleifer, D. Kramer, A. Ben-shaul, W. M. Gelbart, and S.A . Safran, J. Chem. Phys., **92**, 6800 (1990).

[13] L. Foret and A. Wurger, Phys. Rev. Lett., **86**, 5930 (2001)

[14] S. May, D. Harries, and A. Benshaul, Biophys. J., **75**, 159 (1998).

[15] D.Harries, S.May, W.M.Gelbart, and A.Benshaul, Biophys. J. **75**, 159 (1998).

[16] J. O. Raedler, I. Koltover, T. Salditt, and C. R. Safinya, Science **275**, 810 (1997).

[17] I.Koltover, T.Salditt, and C.R.Safinya, Biophys. J., **77**, 915 (1999).